Journal Pre-proof

Regulation of mixed Ag valence state by non-thermal plasma for complete oxidation of formaldehyde

Kai Li , Jian Ji , Yanling Gan , Haibao Huang

PII: S1001-8417(21)00413-7
DOI: https://doi.org/10.1016/j.cclet.2021.06.014
Reference: CCLET 6431

To appear in: *Chinese Chemical Letters*

Received date: 2 March 2021
Revised date: 2 April 2021
Accepted date: 3 June 2021

Please cite this article as: Kai Li , Jian Ji , Yanling Gan , Haibao Huang , Regulation of mixed Ag valence state by non-thermal plasma for complete oxidation of formaldehyde, *Chinese Chemical Letters* (2021), doi: https://doi.org/10.1016/j.cclet.2021.06.014

Communication

<PE-AT>Regulation of mixed Ag valence state by non-thermal plasma for complete oxidation of formaldehyde

Kai Li[a, b], Jian Ji[a, b], Yanling Gan[a, b], Haibao Huang[a, b,*]

[a] *School of Environmental Science and Engineering, Sun Yat-sen University, Guangzhou 510006, China*
[b] *Guangdong Indoor Air Pollution Control Engineering Research Center, Guangzhou 510006, China*

ARTICLE INFO

Article history:
Received 2 March 2021
Received in revised form 2 April 2021
Accepted 27 April 2021
Available online

Keywords:
Ag valence
Non-thermal plasma
HCHO
Complete oxidation
Ag-based catalyst

ABSTRACT

Formaldehyde is an important air pollutant and its removal is essential to protect human health and meet environmental regulations. Ag-based catalyst has a considerable potential for HCHO oxidation in low temperature range. The valence state of Ag is one of the key roles in formaldehyde catalytic oxidation. However, its effect on activity is still ambiguous. Non-thermal plasma and conventional calcination were employed to regulate Ag valence state in this study. Three Ag-Co/CeO_2 catalysts with totally different distribution of Ag species were obtained. A special mixed Ag valence state, ~50% $Ag^{\delta+}$ with a few Ag^0 and Ag^+, was achieved by plasma activation. It had the merits of both good activity and stability. A close relationship between Ag valence state and the activity for HCHO oxidation was established. The activity of different Ag species follows the order: $Ag^{\delta+}$ + Ag^0 + Ag^+ > $Ag^{\delta+}$ > Ag^0 > Ag^+.

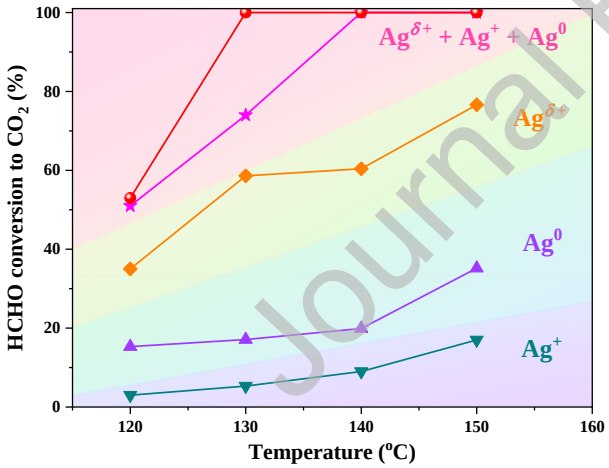

Ag valence state was regulated by plasma activation for complete oxidation of formaldehyde. A close relationship between Ag valence state and the activity for HCHO oxidation was established, and the activity of different Ag species follows the order: $Ag^{\delta+}$ + Ag^0 + Ag^+ > $Ag^{\delta+}$ > Ag^0 > Ag^+.

* Corresponding author.
E-mail address: seabao8@gmail.com (H. Huang)

Formaldehyde is an important air pollutant with strong irritating smell and mainly comes from decorating materials [1-3]. It has serious adverse effects on human health due to its carcinogenic and teratogenic characteristics. It also causes edema, eye irritation, headaches and allergic dermatitis. Therefore, its removal is essential to protect human health and meet environmental regulations. Complete catalytic oxidation of formaldehyde is an attractive technology because of its high effectiveness in achieving total conversion of formaldehyde into harmless carbon dioxide and water directly. Supported noble metal catalyst attracts much attention because of its excellent low-temperature activity for HCHO oxidation [4-9]. Among them, Ag has a much lower price than others, which implies the wild application prospects. However, its activity for HCHO oxidation was poorer. The lowest temperature of 45°C for HCHO complete oxidation was reported recently [10], suggesting Ag-based catalyst has a considerable potential for HCHO removal in the low temperature range or even at room temperature. Therefore, Ag-based catalyst for HCHO oxidation in low temperature becomes one of the current hot topics.

The valence state of Ag is one of the key roles in catalytic oxidation of formaldehyde and relates to the catalytic activity directly. However, it is still ambiguous to identify which one predominates the activity. Metallic Ag is often considered to be favorable for oxygen activation and contributes to good activity for HCHO oxidation [11-15]. Ag^{+} was also proved to dominate the activity [16, 17]. Chen *et. al.* [18] suggested the effects of metallic Ag and Ag^{+} could be distinguished in different temperature ranges. Metallic Ag was primarily responsible for HCHO oxidation at temperature over 140 °C, while Ag_2O species contributed to HCHO oxidation in the temperature below 140 °C. However, both metallic Ag and Ag^{+} were reported to achieve complete oxidation of formaldehyde at temperature below 80 °C [10]. In addition, a partially oxidized Ag species, $Ag^{\delta+}$ ($0 < \delta < 1$), was suggested to contribute a better activity compared with metallic Ag [19-21]. In this context, the effect of Ag valence state on the activity for HCHO oxidation is still unclear and requires deep investigation.

In order to verify the relationship between Ag valence state and the activity for HCHO oxidation, non-thermal plasma and conventional calcination were employed to activate Ag-based catalyst in this study. Non-thermal plasma consists of electrons, ions, molecules, radicals, photons, and excited species, which are all active species for catalyst preparation and treatment. It allows the production of structures and induce processes at surfaces more efficiently in a more controlled way, in comparison with traditional thermal method [22-24]. It worked as an efficient method for Pd-based catalyst activation in our previous work [25, 26]. In this work, conventional calcination, oxygen and hydrogen plasma were employed to achieve catalysts with different Ag valence state. The effect of Ag valence state on HCHO catalytic oxidation activity and stability were discussed. A close relationship between the Ag valence state and HCHO catalytic oxidation activity was established. Various characterizations were applied to investigate the properties of Ag-based catalysts.

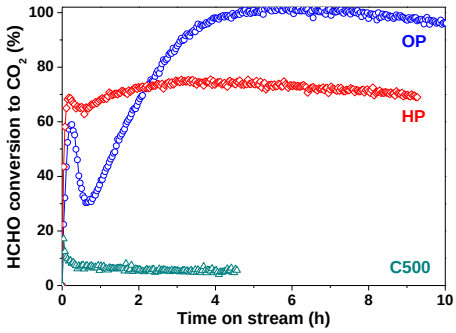

Fig. 1. HCHO conversion to CO_2 over Ag-Co/CeO_2 catalysts with time on stream.

The activity of Ag-Co/CeO_2 catalyst for HCHO complete oxidation was evaluated. The only product is CO_2, suggesting the complete oxidation of HCHO to CO_2 could be achieved over Ag- Co/CeO_2 catalyst. The variation of HCHO conversion to CO_2 with time on stream at reaction temperature of 130 °C is illustrated in Fig. 1. The HCHO conversion of conventional calcined (C500), hydrogen (HP) and oxygen (OP) plasma activated samples exhibited totally different tendencies with time. C500 sample had a low but stable activity except the initial quick jump. It attained an initial conversion of 17% and a stabilized conversion of only 5%.

Plasma activated HP and OP samples exhibited much higher activities than C500. HP sample possessed the merits of both good stability and high activity. Its HCHO conversion reached 69% quickly and kept at around 74% for 9 h. OP sample suffered an activation process before reaching stable. It obtained an initial conversion of 59%, then underwent a 4 h activation process to reach 100% conversion and finally maintained at over 96% for 6 h. The HCHO conversions exhibited the same tendency with time on stream for each sample in the whole temperature range of 120-150 °C, as shown in Fig. S1 (Supporting information). The activation process for OP sample could be accelerated as temperature lifted. That was over 10 h at reaction temperature of 120 °C and could be shortened to half hour with temperature increasing to 150 °C.

For HP, OP and C500 catalysts, the BET surface area exhibited no obvious changes, as shown in Fig. S2 (Supporting information). The diffraction patterns of Co_3O_4 are observed from X-ray diffraction patterns (XRD), as shown in Fig. S3 (Supporting information). This indicates the Co_3O_4 could be formed after both plasma activation and calcination. Those peaks intensities of HP and OP samples are much weaker than C500, implying poor crystallinity of plasma activated samples. However, no diffraction peaks corresponding to Ag species could be distinguished for all samples. Ag and Co could be easily distinguished at the catalyst surface from HRTEM images for all catalysts, as shown in Fig. S4 (Supporting information).

Fig. S5 (Supporting information) displays the Raman spectra of Ag-Co/CeO_2 catalysts. For fresh sample, only two peaks are observed. The strong bond at 461 cm^{-1} corresponds to the fluorite F_{2g} mode of ceria. The peak at 1043 cm^{-1} is due to the presence of nitrate ions [27]. This suggests the existence of silver and cobalt nitrates after impregnation since no further calcination or reduction process was conducted. The nitrate peak disappeared completely for HP and C500 samples. While it still existed along with a declination of intensity for OP sample, indicating the incomplete decomposition of nitrate species. After both plasma activation and calcination, four new peaks occurred. The peaks at 483, 524 and 689 cm^{-1} correspond to the E_g, F_{2g} and A_{1g} symmetries of Co_3O_4, respectively [11,28]. This implies the formation of Co_3O_4, which is consistent with XRD result. The band at 557 cm^{-1} could be attributed to the formation of oxygen vacancy after plasma activation and calcination [29, 30].

Fig. S6 (Supporting information) shows the IR spectra of CeO_2 and Ag-Co/CeO_2 catalysts. Four intense bands in the 1000-1800 cm^{-1} region are observed on ceria surface. The bands at 1065 and 1340 cm^{-1} could be ascribed to the unidentate carbonate species, and the band at 1535 cm^{-1} is due to carboxylate species [31,32]. The band centered at 1630 cm^{-1} could be assigned to the deformation vibration of water. The broad absorbance at 2700-3700 cm^{-1} is attributed to the stretching vibration of OH groups and adsorbed water. After supporting Ag and Co nitrates, the bands in 1000-1600 cm^{-1} region are due to the superposition of carbonate, carboxylate and nitrate species. The bands at 1325 and 1455 cm^{-1} could be ascribed to the asymmetric stretch of nitrate species, and the band at 1040 cm^{-1} is the symmetric stretch of nitrate species [33]. This result indicates the existence of silver and cobalt nitrates over fresh catalyst. After oxygen plasma treatment, only trace of nitrate species could be observed. The species distribution over HP sample was the same as ceria and nitrate species completely disappeared. This suggests both silver and cobalt nitrates species could be decomposed quickly and efficiently by plasma activation in a very short time. And hydrogen plasma is more efficient for nitrate decomposition than oxygen. After 500 °C calcination, all the surface species entirely disappeared and nothing could be observed, suggesting the complete decomposition of nitrates and removal of carbonate, carboxylate and water species during high temperature process.

Fig. S7 (Supporting information) illustrates the H_2-TPR profiles of Ag-Co/CeO_2 catalysts. For fresh Ag-Co/CeO_2 catalyst, two peaks at 177 and 280 °C are observed. The peak at 177 °C is due to the consumption of hydrogen and the formation of NO_2, corresponding to the reduction and decomposition of silver and cobalt nitrates. This could be proved by mass spectra result as shown in Fig. S7b. An intensive peak of nitrogen dioxide at 177 °C formed along with the consumption of hydrogen at the same time, indicating the existence of both reduction and decomposition processes in hydrogen atmosphere. While only hydrogen consumption was observed and no nitrogen dioxide formed at 280 °C. This suggests both silver and cobalt nitrates could be consumed entirely at 177 °C, and the peak at 280 °C is only due to the reduction of cobalt oxide. For plasma activated HP and OP samples, a main reduction peak at 273 °C belonging to the reduction of Co_3O_4 is observed. Two small peaks at 165 and 179 °C ascribed to the reduction of remained nitrates are observed over OP sample. This implies the incomplete decomposition of nitrate exists. For C500, only one reduction peak of Co_3O_4 is observed, suggesting the complete decomposition of nitrates under high temperature calcination. Moreover, its position moves to a higher temperature of 387 °C than others. This could be ascribed to its higher crystallinity degree of Co_3O_4, which could be proved by XRD results. In addition, a reduction peak at high temperature of 754 °C ascribed to reduction of bulk ceria is observed for all samples.

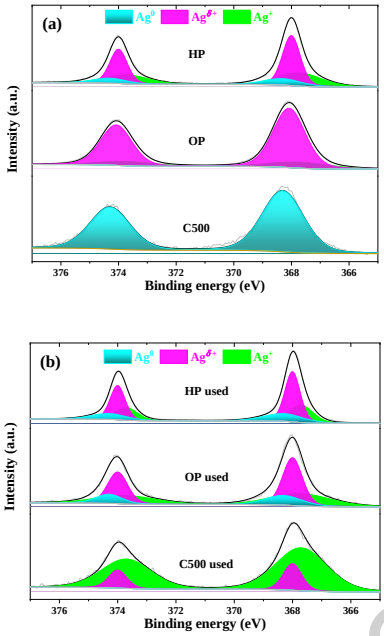

Fig. 2. Ag 3d XPS spectra for (a) fresh and (b) used Ag-Co/CeO_2 catalysts.

Table 1 The content of Ag species of fresh and used Ag-Co/CeO_2 samples from XPS analyses.

Sample	Ag valence	Fresh	Used	
			130 °C	150 °C
HP	1+	33	28	36
	δ+	53	52	54
	0	14	20	10
OP	1+	15	36	25
	δ+	85	47	52
	0	-	17	23
C500	1+	-	82	100
	δ+	-	18	-
	0	100	-	-

X-ray photoelectron spectroscopy (XPS) analysis of Ag 3d was performed and the results are shown in Fig. 2 and Table 1. For HP and OP samples, the binding energies of Ag $3d_{5/2}$ locate at 368.0 eV, which is in the middle of Ag^0 (368.3 eV) and Ag_2O (367.7 eV) [34,35]. It is hard to assign that to either metallic silver or oxidized silver. And it is also impossible to deconvolve it into those two peaks. This indicates the existence of an intermediate valence state between Ag^0 and Ag^+, *i.e.,* $Ag^{\delta+}$ ($0 < \delta < 1$) species, which has been reported in literatures [19-21]. HP, OP and C500 samples showed totally different distribution of Ag species. OP sample contained mainly $Ag^{\delta+}$, HP possessed a mixed valence state of three Ag species and C500 only had metallic Ag. This result hints the totally different characteristics of catalyst pretreatment method. The long-time high temperature calcination could obtain complete decomposition of silver nitrate and forms pure metallic Ag species. Non-thermal plasma works in a much quicker

but milder way since it is characterized by high electron temperature and low gas temperature (close to room temperature). Its reduction process is much milder than high temperature calcination. Therefore, the short-time (5 min) plasma activation could achieve partially reduced Ag species. For oxygen plasma, the Ag species could only be reduced to $Ag^{\delta+}$ species. A component of 85% $Ag^{\delta+}$ and 15% Ag^{+} was attained. Hydrogen plasma has a stronger reducibility, metallic Ag could be formed. Then HP sample obtained a mixed valence state with a component of 14% Ag^{0}, 53% $Ag^{\delta+}$ and 33% Ag^{+}. The Ag^{+} species over HP catalyst resulted from the re-oxidization of reduced Ag via the interaction between Ag and Co_3O_4/CeO_2, since no nitrate species was detected (proved by H_2-TPR, IR and Raman spectra).

These three catalysts also exhibited totally different characteristics during reaction test at 130 °C, as shown in Fig. 2b. The Ag species distribution almost kept unchanged for HP sample after reaction test, whereas big changes were observed for OP and C500 samples. For OP sample, the percentage of $Ag^{\delta+}$ significantly dropped from 85% to 47%, and the percentages of Ag^{+} and metallic Ag increased from 15% and 0% to 36% and 17%, respectively. For C500, metallic Ag disappeared and was oxidized completely. The percentages of Ag^{+} and $Ag^{\delta+}$ increased to 82% and 18%, respectively. Furthermore, similar Ag species distributions were observed for used samples after testing at 150 °C, as shown in Fig. S8 (Supporting information) and Table 1. It still remained unchanged for HP sample. A complete oxidation to Ag^{+} was observed for C500. A component of 52% $Ag^{\delta+}$, 23% Ag^{0} and 25% Ag^{+} over OP sample was attained.

Obviously, a special mixed Ag valence state, *i.e.,* ~50% $Ag^{\delta+}$ with a few Ag^{0} and Ag^{+}, could be proposed. HP sample had this special mixed Ag valence state and did not change even after long-time reaction test at both 130 and 150 °C. Though fresh OP sample owned mainly $Ag^{\delta+}$ species, it could reach this special state finally after *in situ* activation process at both 130 and 150 °C. While C500 sample never had it. Ag valence state could be highly affected by its surrounding environment, especially the redox cycles of Co^{2+}/Co^{3+} and Ce^{3+}/Ce^{4+} [36-38]. The Co was essential to the activity since the HCHO conversion was only 38% for the HP sample without Co loading at 150 °C. It could surely improve the catalytic activity. However, it hardly affected the Ag valence state. The ratio of $Co^{2+}/(Co^{2+} + Co^{3+})$ for HP, OP and C500 sample was 87%, 72% and 79%, respectively, as shown in Fig. S9 and Table S1 (Supporting information). All of them approached to 80% after reaction test (both 130 and 150 °C). The ratio of $Ce^{3+}/(Ce^{3+} + Ce^{4+})$ for HP, OP and C500 sample was 24%, 17% and 31% respectively, as shown in Fig. S10 and Table S2 (Supporting information). All of them approached to 31% after reaction test (both 130 and 150 °C). Plasma activated samples had different Co^{2+} and Ce^{3+} contents before and after reaction test, while C500 attained the same contents. In this case, the contribution of Co and Ce could be excluded and the special mixed Ag valence state was predominated by plasma activation.

The XPS analyses are consistent with HCHO conversion (Fig. 1 and Fig. S1). HP sample had stable conversion and Ag valence state. OP sample underwent activation process and could also reach stable activity and Ag valence state. C500 sample exhibited quick deactivation and achieved stable activity and Ag valence state. In this context, a relationship between Ag valence state and HCHO conversion was established to deep understand the contribution of Ag species, as shown in Fig. 3. The mixed valence state of $Ag^{\delta+}$ + Ag^{0} + Ag^{+} contributed to the stabilized activity of HP and OP samples. $Ag^{\delta+}$ and Ag^{0} species were responsible for the initial conversions of OP and C500. Ag^{+} species contributed to the stabilized conversion of C500. Apparently, the activity of HCHO catalytic oxidation of different Ag species follows the order: $Ag^{\delta+}$ + Ag^{0} + Ag^{+} > $Ag^{\delta+}$ > Ag^{0} > Ag^{+}. The mixed valence state of $Ag^{\delta+}$+ Ag^{0} + Ag^{+} had the merits of both good activity and stability. $Ag^{\delta+}$ species also had good activity, whereas its stability was really poor and a quick deactivation could be observed. Ag^{0} species contributed to a much lower activity and poorer stability. Ag^{+} species had a stable but the lowest conversion.

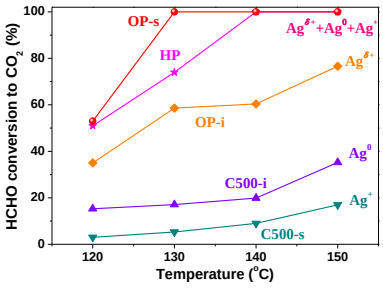

Fig. 3. The effect of Ag valence state on HCHO conversion with temperature. The postfix letters of i and s denote the initial and stabilized conversions, respectively.

The activation of oxygen is often considered as one of the important rate-limiting steps in HCHO catalytic oxidation [39,40]. The valence state of Ag plays a very important role in oxygen activation. The oxygen activation is dependent on the redox cycles of Ag^0/Ag^+ [11]. Metallic Ag is generally considered to be favorable for oxygen activation. This view was partially proved in this study. However, Ag^0 species is not stable enough and could be easily oxidized to Ag^+ during reaction test. Thus, the balance of Ag^0/Ag^+ redox cycle could be broken. Ag^+ species is stable but its activity is limited. $Ag^{\delta+}$ ($0 < \delta < 1$) species was suggested to contribute a better activity compared with metallic Ag. It also underwent the disadvantage of unstable. However, Ag redox cycle could be stabilized when intermediate valence state of $Ag^{\delta+}$ inserted. A new redox cycle of $Ag^0/Ag^{\delta+}/Ag^+$ could be established, which could surely improve the ability and stability of oxygen activation, and finally enhanced the activity and stability of HCHO catalytic oxidation significantly.

In summary, conventional C500, plasma activated HP and OP catalysts exhibited totally different distribution of Ag species. HP sample possessed a mixed valence of $Ag^{\delta+} + Ag^0 + Ag^+$, OP contained mainly $Ag^{\delta+}$ and C500 only had metallic Ag. HP and OP samples exhibited much higher activities than conventional C500 catalyst. HP sample possessed the merits of both good stability and high activity. OP sample suffered an activation process before reaching stable. C500 sample had a low but stable activity except the initial quick jump. A close relationship between Ag valence state and the activity for HCHO oxidation was established. The conversion of different Ag species follows the order: $Ag^{\delta+} + Ag^0 + Ag^+ > Ag^{\delta+} > Ag^0 > Ag^+$.

Declaration of interests

The authors declare that they have no known competing financial interests or personal relationships that could have appeared to influence the work reported in this paper.

Acknowledgments

This work was supported by the National Natural Science Foundation of China (NSFC) (Nos. 22006166 and 22076224), the China Postdoctoral Science Foundation (No. 2019M653184), Guangdong Basic and Applied Basic Research Foundation (No. 2020A1515010865) and Fundamental Research Funds for the Central Universities (Nos. 20lgjc03 and 20lgpy95).

References

<bib id="bib1" type="Periodical"><number>[1]</number>B.Y. Bai, Q. Qiao, J.H. Li, et al., Chin. J. Catal. 37 (2016) 102-122.</bib>

<bib id="bib2" type="Periodical"><number>[2]</number>J.Q. Torres, S. Royer, J.P. Bellat, et al., ChemSusChem 6 (2013) 578-592.</bib>

<bib id="bib3" type="Periodical"><number>[3]</number>H.B. Huang, Y. Xu, Q.Y. Feng, et al., Catal. Sci. Technol. 5 (2015) 2649-2669.</bib>

<bib id="bib4" type="Periodical"><number>[4]</number>J. Ye, Y. Yu, J. Fan, et al., Environ. Sci. Nano 7 (2020) 3655-3709.</bib>

<bib id="bib5" type="Periodical"><number>[5]</number>J. Guo, C. Lin, C. Jiang, et al., Appl. Surf. Sci. 475 (2019) 237-255.</bib>

<bib id="bib6" type="Periodical"><number>[6]</number>Q.L. Xu, W.Y. Lei, X.Y. Li, et al., Environ. Sci. Technol. 48 (2014) 9702-9708.</bib>

<bib id="bib7" type="Periodical"><number>[7]</number>L.H. Nie, J.G. Yu, M. Jaroniec, et al., Catal. Sci. Technol. 6 (2016) 3649-3669.</bib>

<bib id="bib8" type="Periodical"><number>[8]</number>S.Y. Huang, B. Cheng, J.G. Yu, et al., ACS Sustainable Chem. Eng. 6 (2018) 12481-12488.</bib>

<bib id="bib9" type="Periodical"><number>[9]</number>B.B. Chen, X.B. Zhu, M. Crocker, et al., Appl. Catal. B 154 (2014) 73-81.</bib>

<bib id="bib10" type="Periodical"><number>[10]</number>L. Zhang, Y. Xie, Y. Jiang, et al., Appl. Catal. B 268 (2020) 118461.</bib>

<bib id="bib11" type="Periodical"><number>[11]</number>B.Y. Bai, J.H. Li, ACS Catal. 4 (2014) 2753-2762.</bib>

<bib id="bib12" type="Periodical"><number>[12]</number>F.L. Yu, Z.P. Qu, X.D. Zhang, et al., J. Energy Chem. 22 (2013) 845-852.</bib>

<bib id="bib13" type="Periodical"><number>[13]</number>B.Y. Bai, Q. Qiao, H. Arandiyan, et al., Environ. Sci. Technol. 50 (2016) 2635-2640.</bib>

<bib id="bib14" type="Periodical"><number>[14]</number>X.Y. Chen, M. Chen, G.Z. He, et al., J. Phys. Chem. C 122 (2018) 27331-27339.</bib>

<bib id="bib15" type="Periodical"><number>[15]</number>C. Ou, C. Chen, T. Chan, et al., J. Catal. 380 (2019) 43-54.</bib>

<bib id="bib16" type="Periodical"><number>[16]</number>L. Ma, C.Y. Seo, X.Y. Chen, et al., Chem. Eng. J. 350 (2018) 419-428.</bib>

<bib id="bib17" type="Periodical"><number>[17]</number>L. Yu, R.S. Peng, L.M. Chen, et al., Chem. Eng. J. 334 (2018) 2480-2487.</bib>

<bib id="bib18" type="Periodical"><number>[18]</number>X. Chen, H. Wang, M. Chen, et al., Appl. Catal. B 282 (2021) 119543.</bib>

<bib id="bib19" type="Periodical"><number>[19]</number>R.M. Fang, M. He, H.B. Huang, et al., Chemosphere 213 (2018) 235-243.</bib>

<bib id="bib20" type="Periodical"><number>[20]</number>Z.W. Huang, X. Gu, Q.Q. Cao, et al., Angew. Chem. Int. Ed. 51 (2012) 4198-4203.</bib>

<bib id="bib21" type="Periodical"><number>[21]</number>P.P. Hu, Z.W. Huang, Z. Amghouz, et al., Angew. Chem. Int. Edit. 53 (2014) 3418-3421.</bib>

<bib id="bib22" type="Periodical"><number>[22]</number>Z. Wang, Y. Zhang, E.C. Neyts, et al., ACS Catal. 8 (2018) 2093-2110.</bib>

<bib id="bib23" type="Periodical"><number>[23]</number>C.J. Liu, M.Y. Li, J.Q. Wang, et al., Chin. J. Catal. 37 (2016) 340-348.</bib>

<bib id="bib24" type="Periodical"><number>[24]</number>L.B. Di, J.S. Zhang, X.L. Zhang, Plasma Process. Polym. 15 (2018) 19.</bib>

<bib id="bib25" type="Periodical"><number>[25]</number>K. Li, J. Ji, M. He, et al., Catal. Sci. Technol. 10 (2020) 6257-6265.</bib>

<bib id="bib26" type="Periodical"><number>[26]</number>K. Li, J. Ji, H. Huang, et al., Chemosphere 246 (2020) 125762.</bib>

<bib id="bib27" type="Periodical"><number>[27]</number>B. Pettinger, X. Bao, I. Wilcock, et al., Angew. Chem. Int. Ed. 33 (1994) 85-86.</bib>

<bib id="bib28" type="Periodical"><number>[28]</number>W. Zhu, X. Chen, J. Jin, et al., Chinese. J. Catal. 41 (2020) 679-690.</bib>

<bib id="bib29" type="Periodical"><number>[29]</number>T. Taniguchi, T. Watanabe, N. Sugiyama, et al., J. Phys. Chem. C 113 (2009) 19789-19793.</bib>

<bib id="bib30" type="Periodical"><number>[30]</number>Z. Wu, M. Li, J. Howe, et al., Langmuir 26 (2010) 16595-16606.</bib>

<bib id="bib31" type="Periodical"><number>[31]</number>C. Li, Y. Sakata, T. Arai, et al., J. Chem. Soc. Faraday T. 85 (1989) 1451-1461.</bib>

<bib id="bib32" type="Periodical"><number>[32]</number>G. Bampos, P. Bika, P. Panagiotopoulou, et al., Appl. Catal. A 588 (2019) 13.</bib>

<bib id="bib33" type="Periodical"><number>[33]</number>K. Hadjiivanov, Catal. Lett. 68 (2000) 157-161.</bib>

<bib id="bib34" type="Periodical"><number>[34]</number>T.C. Kaspar, T. Droubay, S.A. Chambers, et al., J. Phys. Chem. C 114 (2010) 21562-21571.</bib>

<bib id="bib35" type="Periodical"><number>[35]</number>L. Ma, D.S. Wang, J.H. Li, et al., Appl. Catal. B 148 (2014) 36-43.</bib>

<bib id="bib36" type="Periodical"><number>[36]</number>S. Liu, X. Wu, W. Liu, et al., J. Catal. 337 (2016) 188-198.</bib>

<bib id="bib37" type="Periodical"><number>[37]</number>J. Zhang, L. Li, X. Huang, et al., J. Mater. Chem. 22 (2012) 10480-10487.</bib>

<bib id="bib38" type="Periodical"><number>[38]</number>Z.P. Qu, D. Chen, Y.H. Sun, et al., Appl. Catal. A 487 (2014) 100-109.</bib>

<bib id="bib39" type="Periodical"><number>[39]</number>P.P. Hu, Z. Amghouz, Z.W. Huang, et al., Environ. Sci. Technol. 49 (2015) 2384-2390.</bib>

<bib id="bib40" type="Periodical"><number>[40]</number>L. Miao, J. Wang, P. Zhang, Appl. Surf. Sci. 466 (2019) 441-453.</bib>